Defect-enhanced nematic surface order reconstruction

Milan Ambrožič
Engineering Ceramics Department, Jožef Stefan Institute, Jamova 39, 1000 Ljubljana, Slovenia

Samo Kralj
Laboratory of Physics of Complex Systems, Faculty of Natural Sciences and Mathematics, University of Maribor, Koroška 160, 2000 Maribor, Slovenia and Condensed Matter Physics Department, Jožef Stefan Institute, Jamova 39, 1000 Ljubljana, Slovenia

Epifanio G. Virga
Dipartimento di Matematica and CNISM, Università di Pavia, Via Ferrata 1, I-27100 Pavia, Italy
(Received 13 November 2006; published 22 March 2007)

Within the Landau–de Gennes phenomenological theory, we study the influence of an applied electric field with average strength E_a on the position of a nematic line defect with topological charge $M=\pm\frac{1}{2}$ in a hybrid cell. We explore the biaxial structure of the defect core and we describe its expulsion from the cell upon increasing E_a. We show that prior to the expulsion the defect core displays dramatic changes for strong enough surface anchorings. At a critical value of E_a, the core broadens and merges into a surface layer with a large biaxiality. This transition corresponds to the reconstruction of the nematic order already observed in the bulk in response to an applied electric field. A similar order reconstruction could take place even in the absence of defects, but at a higher threshold.

DOI: 10.1103/PhysRevE.75.031708 PACS number(s): 61.30.Gd, 61.30.Jf

I. INTRODUCTION

Defects in uniaxial nematic liquid crystals (LCs) have long attracted interest [1]. Either they appear in response to confining topological constraints or they are caught in metastable states that arise as a result of a continuous symmetry breaking. They play a vital role in new generations of LC devices [2], where defects mediate the switching between states stable in no field. In addition, defects exhibit many universal features that make them attractive from a fundamental point of view [3]. To this regard, it should be noted that the main reason for their existence is that the phase they inhabit is achieved via a symmetry breaking transition, which is commonly encountered in nature. Consequently, it is perhaps not surprising that the first theory of topological defects was developed in cosmology [4].

Topological defects in ordered media are singular regions exhibiting order parameter configurations that cannot be transformed into a homogeneous ground state via continuous deformations. In the uniaxial nematic phase, defects are conventionally classified according to their topological charge M (also called the Frank index) [1]. This topological quantity is determined in terms of the rotation of the nematic director field $\mathbf{n}$ on either surfaces or lines enclosing the defect; it most remarkably reveals the nature of a defect on the macroscopic scale. Within the simple Frank theory [5], which is constructed solely in terms of $\mathbf{n}$, defects correspond to singular regions, where $\mathbf{n}$ is not uniquely defined.

The uniaxial nematic phase exhibits both point and line defects [1]. Commonly observed defects carry a topological charge M of strength either 1 or $\frac{1}{2}$. The former are typically point defects [6], while the latter are line defects. The region where the LC ordering is apparently modified by the presence of a defect is the defect core: it is described by the order tensor $\mathbf{Q}$, which composes in one and the same representation both uniaxial and biaxial states [7]. The notion of topological charge is lost within the defect core, as there the order tensor field $\mathbf{Q}$ is continuous. The topological charge M we assign to a defect is computed for the far nematic field, which is assumed to be uniaxial.

The static core structure of point defects with $M=\pm 1$ is well known [8–12]. It commonly exhibits a biaxial core, characterized by a cylindrically symmetric, ringlike structure [13,14]. The transverse cross section of the ring associated with a point defect with charge $M=\pm 1$ has the same structure as a line defect with $M=\pm\frac{1}{2}$ [15].

The structure, position, and very existence of a defect can be controlled by external fields. In confined geometries with weak anchoring conditions, defects could be expelled under sufficiently strong fields without any structural change [16,17]. It has also been shown that external fields can affect the core structure of defects [18,19] and either stabilize or destabilize different defect configurations [2,20]. Defects can mediate structural changes [2] in confined LCs and strongly affect the field threshold that triggers structural transitions. It was further studied in detail how a line defect can be expelled for a weak enough anchoring [21] and the variation of the defect core structure on approaching a surface [22].

In this work we study the influence of an external electric field on a nematic line defect with $M=-\frac{1}{2}$ within a hybrid, planar cell [23]. The electric field tends to expel the defect from the cell, whereas a surface anchoring condition opposes this tendency. We calculate the critical field for the defect expulsion as a function of the anchoring strength. We show that for strong enough anchoring strengths the defect expulsion happens in two stages: first, the line defect explodes into a plane defect close to the antagonistic boundary; then, the plane defect leaves the cell. The former stage involves an order reconstruction in a boundary layer, which in the presence of the defect takes place earlier than in its absence.

The plan of the paper is as follows. In Sec. II, we introduce the phenomenological model that we employ and we describe the geometry of the problem and our parametrization. In Sec. III, we present the results of our study. In the last section we collect our conclusions. Some technical details are recorded in the closing Appendix.

II. MODEL

A. Free energy

We use the Landau–de Gennes [7] phenomenological description of the mesoscopic nematic ordering given in terms of a symmetric, traceless tensor [24]

$$\mathbf{Q} = \sum_{i=1}^{3} \lambda_i \mathbf{e}_i \otimes \mathbf{e}_i. \tag{1}$$

Here λ_i and $\mathbf{e}_i$ are the ith eigenvalue and the ith eigenvector of $\mathbf{Q}$, respectively. In case of relatively weak distortions, the system exhibits a uniaxial ordering, which is represented by

$$\mathbf{Q} = S\left(\mathbf{n} \otimes \mathbf{n} - \frac{1}{3}\mathbf{I}\right). \tag{2}$$

The unit vector $\mathbf{n}$, also called the nematic director, points along the local uniaxial ordering direction. The uniaxial order parameter S quantifies the extent of fluctuations about this direction.

The degree of biaxiality is measured by the biaxiality parameter β^2, defined as [25]

$$\beta^2 := 1 - \frac{6(\mathrm{tr}\mathbf{Q}^3)^2}{(\mathrm{tr}\mathbf{Q}^2)^3}. \tag{3}$$

It ranges in the interval [0,1]. The value $\beta^2=0$ represents a uniaxial ordering and $\beta^2=1$ an ordering with the maximum degree of biaxiality. Note that $\mathrm{tr}\mathbf{Q}^3$ is related to the determinant of $\mathbf{Q}$ through the relation $\mathrm{tr}\mathbf{Q}^3=3\det\mathbf{Q}$. Therefore the maximal biaxiality criterion $\beta^2=1$ coincides with the condition that $\det\mathbf{Q}=0$, which further implies that at least one eigenvalue λ_i equals zero.

We express the free energy of the confined nematic phase

$$\Omega := \int \sigma_V dV + \int \sigma_S dS$$

as the sum of a volume integral and a surface integral; the corresponding densities are $\sigma_V=\sigma_b+\sigma_e+\sigma_f$ and σ_S, with

$$\sigma_b = \frac{A}{2}\mathrm{tr}\mathbf{Q}^2 - \frac{B}{3}\mathrm{tr}\mathbf{Q}^3 + \frac{C}{4}(\mathrm{tr}\mathbf{Q}^2)^2, \tag{4a}$$

$$\sigma_e = \frac{L}{2}|\nabla\mathbf{Q}|^2, \tag{4b}$$

$$\sigma_f = -\frac{\varepsilon_0}{2}\mathbf{E}\cdot\varepsilon\mathbf{E}, \tag{4c}$$

$$\sigma_S = \frac{W}{2}\mathrm{tr}(\mathbf{Q}-\mathbf{Q}_s)^2. \tag{4d}$$

The bulk term σ_b enforces the uniaxial ordering described by Eq. (2), where the equilibrium order parameter is given by

$$S_{\mathrm{eq}}(T) = \frac{B}{4C}\left(1 + \sqrt{1 - \frac{24AC}{B^2}}\right). \tag{5}$$

The temperature T enters the model through the coefficient $A=A_0(T-T_*)$, where T_* is for the *supercooling* temperature and A_0, B, C are material constants. The elastic term σ_e penalizes the deviations from a spatially homogeneous texture of $\mathbf{Q}$. For simplicity, we limit attention to the approximation of equal nematic elastic constants [7], where the elasticity of the system is represented solely by $L>0$.

The presence of an external electric field $\mathbf{E}=-\nabla U$, where U is the electrostatic potential, gives rise to the free energy density σ_f. The quantity ε_0 is the electric permeability constant and ε is the dielectric tensor, which describes the local anisotropic response of the nematic ordering to $\mathbf{E}$. One commonly expresses ε as [24]

$$\varepsilon = \varepsilon_i\mathbf{I} + \varepsilon_a\mathbf{Q}, \tag{6}$$

where ε_i and ε_a are the isotropic and anisotropic dielectric susceptibilities. We limit ourselves to consider liquid crystals with $\varepsilon_a>0$, which favor a nematic uniaxial ordering along $\mathbf{E}$. With this in mind, we rewrite σ_f in the following form:

$$\sigma_f = -\frac{\varepsilon_0}{2}(\varepsilon_i|\nabla U|^2 + \varepsilon_a \nabla U\cdot\mathbf{Q}\nabla U). \tag{7}$$

The interaction at the interface between the LC body and the bounding surfaces is described by the surface anchoring density σ_s. Its strength is measured by the positive anchoring constant W. The surface term favors locally an ordering described by $\mathbf{Q}_s$, the form of which depends on the surface preparation.

B. Geometry of the problem and parametrization

We consider a nematic liquid crystal confined within a cell between two plane, parallel plates at the distance $d_z := 2d$, as shown in Fig. 1. The plates are placed at $z=\pm d$ of a Cartesian coordinate system. The coordinate axes (x,y,z) point along the unit vectors $(\mathbf{e}_x,\mathbf{e}_y,\mathbf{e}_z)$, respectively. We apply the voltage $2U_a$ across the cell, i.e., the applied electrical potential is U_a at the top plate and $-U_a$ at the bottom plate. The average electric field within the cell is thus $\mathbf{E}_a=-E_a\mathbf{e}_z$ with $E_a := U_a/d$; it promotes the uniaxial alignment of the nematic director along the z axis. The top plate enforces a homeotropic anchoring. On the contrary, the bottom plate enforces a homogeneous, tangential anchoring along the y axis. The lengths d_x and d_y of the cell's plates along the x and y axes are much larger than d $(d_x \sim d_y \gg d)$.

These boundary conditions are compatible with the germination of a line defect with topological charge $M=-\frac{1}{2}$. In the simulation, we study the position of this line defect as a function of E_a. The defect is parallel to the x axis of the simulation cell and the origin of the defect core is the point

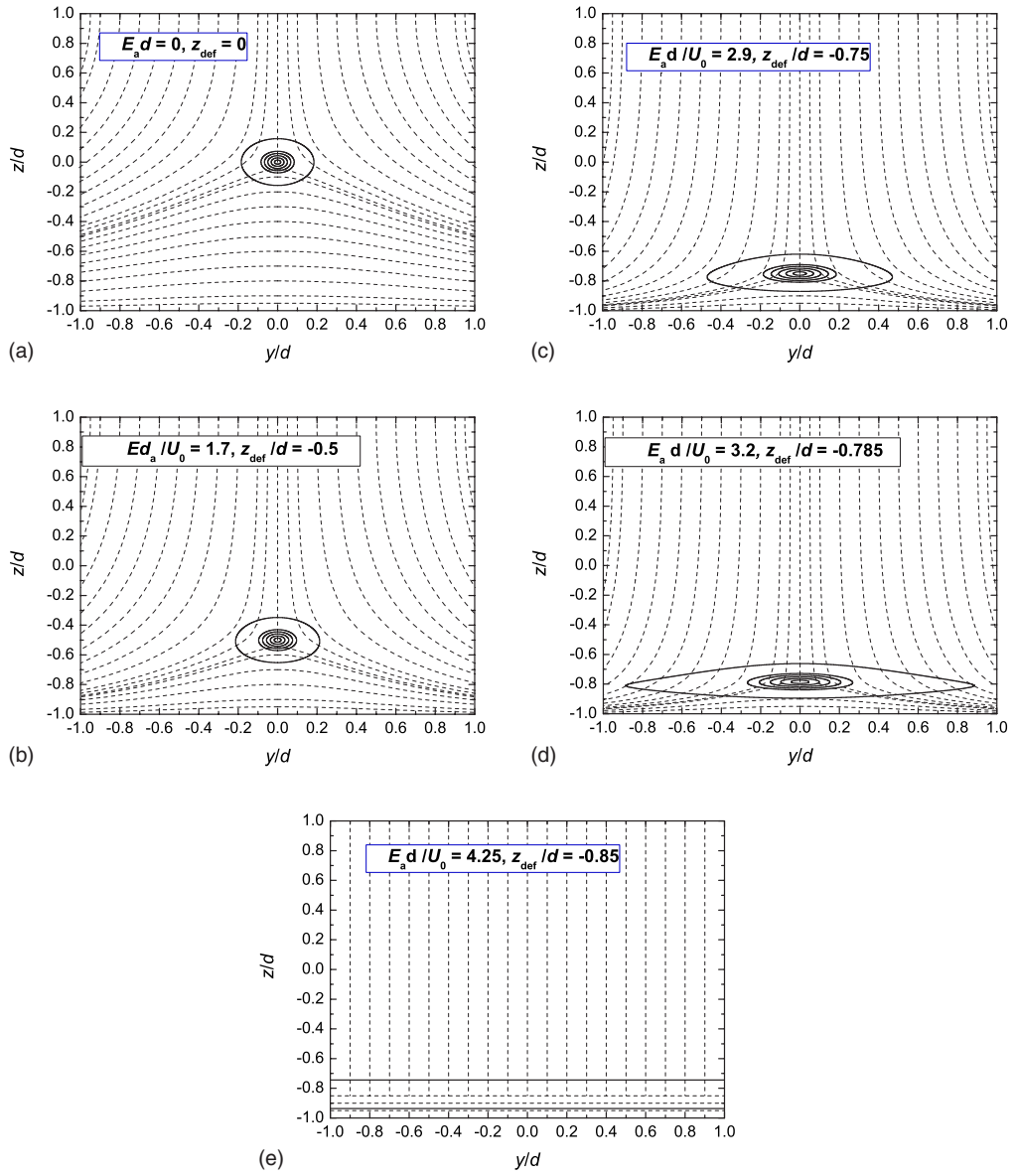

FIG. 1. (Color online) The geometry of the problem and the nematic texture for different values of E_a. The cell's plates are at $z=\pm d$. The director field profile (dashed lines) and the contour plot of r (solid lines from inside the defect toward the bulk: $r/q_0=0.1$, 0.2, 0.3, 0.4, 0.5, and 1) for different values of $E_a<E_c$: (a) $E_a=0$, $z_{\mathrm{def}}=0$; (b) $E_a d/U_0\approx 1.7$, $z_{\mathrm{def}}/d=-0.5$; (c) $E_a d/U_0\approx 2.9$, $z_{\mathrm{def}}/d=-0.75$; (d) $E_a d/U_0\approx 3.2$, $z_{\mathrm{def}}/d=-0.785$; (e) $E_a d/U_0=4.25$, $z_{\mathrm{def}}/d=-0.85$. In the last texture the line defect has already grown into the biaxial layer (only the pair of solid lines corresponding to $r/q_0=1$ are shown). $W/W_0=5$, $d/\xi_b=4$.

$(y_{\mathrm{def}}, z_{\mathrm{def}})$ in the (y,z) plane. The results we shall obtain also apply to a line defect with $M=\frac{1}{2}$, equally compatible with the imposed boundary conditions.

We consider nematic distortions enjoying the mirror symmetry with respect to the (x,z) plane at $y=0$, and with the eigenvalues λ_i independent of the x coordinate. We further study textures in which one eigenvector of $\mathbf{Q}$ always points along $\mathbf{e}_x$. Therefore we assume that $\mathbf{Q}=\mathbf{Q}(y,z)$ and $y_{\mathrm{def}}=0$. It is convenient to introduce the following parametrization [26]

$$\mathbf{Q} = -2q_1\mathbf{e}_x\otimes\mathbf{e}_x + (q_1-q_2)\mathbf{e}_y\otimes\mathbf{e}_y + (q_1+q_2)\mathbf{e}_z\otimes\mathbf{e}_z + q_3(\mathbf{e}_y\otimes\mathbf{e}_z + \mathbf{e}_z\otimes\mathbf{e}_y). \tag{8}$$

The scalar parameters q_i are related to the eigenvalues of $\mathbf{Q}$ through the equations $\lambda_1=-2q_1$, $\lambda_2=q_1-\sqrt{q_2^2+q_3^2}$, and $\lambda_3=q_1+\sqrt{q_2^2+q_3^2}$. It is well known that the axis of the defect core is marked by the exchange of two eigenvalues [15]. In our setting, this exchange is characterized by $\lambda_2=\lambda_3$, which requires that

$$r := \sqrt{q_2^2+q_3^2} \tag{9}$$

vanishes. The off-diagonal term q_3 represents the rotation of the eigenframe of $\mathbf{Q}$ in the (y,z) plane with respect to the cell's frame. The defect core is essentially biaxial. However, away from it, the texture is almost uniaxial and can approximately be described by the director field

$$\mathbf{n} = \cos\varphi \mathbf{e}_y + \sin\varphi \mathbf{e}_z, \tag{10}$$

where

$$\tan 2\varphi := -\frac{q_3}{q_2}. \tag{11}$$

C. Scaling and boundary conditions

In addition to the cell width d_z, the other important lengths entering the problem are the biaxial correlation length ξ_b, the field coherence length ξ_f, and the surface extrapolation length d_e. The biaxial correlation length estimates the size of the defect core. If $d/d_e \gtrapprox 1$ $(d/\xi_f \gtrapprox 1)$ then the anchoring condition (external field) strongly influences the orientational ordering. Following conventional definitions [7], we express these lengths as

$$\xi_b := \sqrt{\frac{L}{BS_{\mathrm{eq}}}}, \quad \xi_f := \sqrt{\frac{L}{\varepsilon_0 \varepsilon_a E_a^2}}, \quad d_e := \frac{L}{W}. \tag{12}$$

For scaling purposes we introduce the dimensionless reduced temperature θ as

$$\theta := \frac{T - T_*}{T_{**} - T_*}, \tag{13}$$

where

$$T_{**} := T_* + \frac{B^2}{24A_0C}$$

is the superheating temperature. In the interval $\theta \in [0,1]$ the liquid crystal possesses metastable states and the isotropic-nematic transition takes place at $\theta = 8/9$.

We scale the order parameters to

$$q_0 := \frac{B}{4C} = S_{\mathrm{eq}}(T_{**})$$

as $\tilde{q}_i = q_i/q_0$, $i=1,2,3$. In this scaling the equilibrium ordering $\tilde{s} = S_{\mathrm{eq}}/q_0$ is expressed as

$$\tilde{s} = 1 + \sqrt{1-\theta} =: t,$$

and similarly $\tilde{r} = r/q_0$. We introduce the bare biaxial correlation length as

$$\xi_0 := \sqrt{\frac{L}{Bq_0}} = \xi_b \sqrt{t},$$

and the quantities

$$\Omega_0 := \frac{B^4 d_x d_y d}{64C^3}, \quad \tilde{\varepsilon}_a := \frac{\varepsilon_a q_0}{\varepsilon_i}, \quad \text{and } U_0 := q_0 \sqrt{\frac{2L}{t\varepsilon_i \varepsilon_0}}.$$

Using them, we define the following dimensionless quantities: $\tilde{\Omega} = \Omega/\Omega_0$, $\tilde{U} = U/U_0$, $\tilde{W} = \frac{\xi_0^2}{dd_e} = W/W_0$, with $W_0 := q_0 Bd$. We further scale all the lengths in units of d, i.e., $\tilde{y} = y/d$, $\tilde{z} = z/d$, and $\tilde{\xi}_0 = \xi_0/d$. For briefness, we henceforth omit the tildes. With these definitions we obtain the following expressions for the dimensionless free energy densities

$$\sigma_b = \frac{\theta}{6}(3q_1^2 + q_2^2 + q_3^2) + 2q_1(q_1^2 - q_2^2 - q_3^2) + \frac{1}{4}(3q_1^2 + q_2^2 + q_3^2)^2, \tag{14a}$$

$$\sigma_e = \xi_0^2 (3q_{1,y}^2 + q_{2,y}^2 + q_{3,y}^2 + 3q_{1,z}^2 + q_{2,z}^2 + q_{3,z}^2), \tag{14b}$$

$$\sigma_f = -\frac{\xi_0^2}{t}\{U_{,y}^2 + U_{,z}^2 + \varepsilon_a [U_{,y}^2 (q_1 - q_2) + 2U_{,y}U_{,z}q_3 + U_{,z}^2 (q_1 + q_2)]\}, \tag{14c}$$

$$\sigma_S = W[3q_1^2 + q_2^2 + q_3^2 + 3q_{s1}^2 + q_{s2}^2 + q_{s3}^2 - 2(3q_1 q_{s1} + q_2 q_{s2} + q_3 q_{s3})], \tag{14d}$$

where $q_{i,j}$ and $U_{,j}$ denote derivatives with respect to the j coordinate. In σ_S we expressed the preferred surface order tensor $\mathbf{Q}_s$ as $\mathbf{Q}$ in Eq. (8) with q_i replaced by q_{si}, for $i=1,2,3$.

In the scaling employed here, the uniaxial ordering is represented by the triple

$$\{q_1, q_2, q_3\} = \left\{\frac{t}{6}, -\frac{t\cos 2\varphi}{2}, \frac{t\sin 2\varphi}{2}\right\}.$$

Accordingly, at the upper plate we enforce the uniaxial homeotropic anchoring represented by $\varphi = \frac{\pi}{2}$ and $\{q_{s1}, q_{s2}, q_{s3}\} = \{\frac{t}{6}, \frac{t}{2}, 0\}$. At the bottom plate we enforce the uniaxial tangential anchoring represented by $\varphi = 0$ and $\{q_{s1}, q_{s2}, q_{s3}\} = \{\frac{t}{6}, -\frac{t}{2}, 0\}$. The anchoring strength is set equal to W at both plates.

We obtain the Euler-Lagrange equations as stationary conditions for the total free energy of the system: they are recorded in the Appendix. These equations were solved numerically by using the over-relaxation method [27].

In our numerical simulations we follow the position z_{def} of the line defect as a function of the average applied field E_a. We initially set the defect at the center of the cell for $E_a = 0$. The defect is stabilized within the cell for $W \gtrapprox 0.3$. The conditions at the bounding plates are enforced by the appropriate surface equilibrium equations at $z = \pm d$. On the lateral walls at $y = \pm d_y/2$, we prescribe free boundary conditions. We varied the value of d_y to identify the behavior of the equilibrium configuration in the limit as $d_y \to \infty$.

III. RESULTS

The simulations were carried out in the deep nematic phase. The scaled temperature is set equal to $\theta = -8$, corresponding to $t=4$ and $\xi_0 = 2\xi_b$. Further we set $\varepsilon_a q_0/\varepsilon_i = 0.3$, and we consider cells of thickness $d_z = 8\xi_b$ and $d_z = 16\xi_b$.

We first focus on the defect structure for $E_a = 0$. Except for very weak anchorings (i.e., for $W/W_0 \lessapprox 0.3$), where a homogeneous, defect-less texture has lower free energy than a defective texture, the defect is stabilized in the center of the cell, see Fig. 1(a). We indicate with dashed lines the orientation of the principal eigenvector of the tensor $\mathbf{Q}$ determined by Eq. (11). The defect core is represented by the contour plot in the (y,z) plane of the function $r = r(y,z)$ defined in

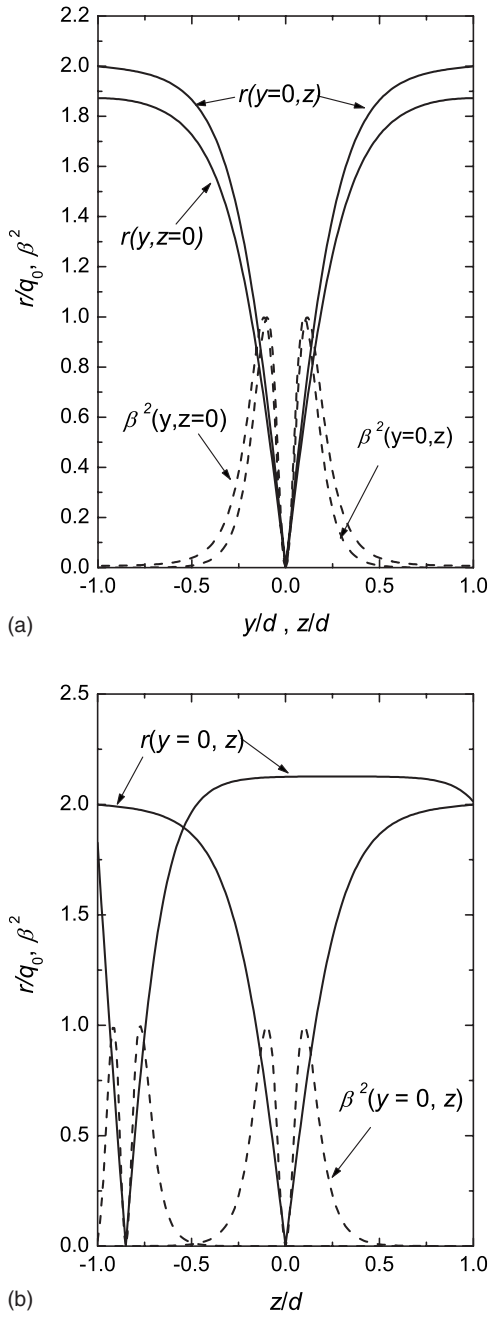

FIG. 2. Plots of $r(y_{\mathrm{def}},z)$, $r(y,z_{\mathrm{def}})$, $\beta^2(y_{\mathrm{def}},z)$, and $\beta^2(y,z_{\mathrm{def}})$ revealing the core structure of the line defect. For $E_a \ll E_c$, these graphs evoke circular profiles in the corresponding contour plot in the (y,z) plane. The departure from such a circular symmetry becomes apparent when the defect separation from the plate is comparable with ξ_b. (a) Comparison between the y and z dependencies of the core structure for $z_{\mathrm{def}}=0$ reveals a slight asymmetry, (b) Comparison between the core structures for $z_{\mathrm{def}}=0$ (right) and $z_{\mathrm{def}}=-0.85$ (left). $W/W_0=5$, $d/\xi=4$.

Eq. (9). At the given temperature, one finds that $r \sim 2q_0$ far away (in terms of ξ_b) from the defect center. On approaching the defect, r monotonically decreases and equals zero at its axis. A more detailed analysis of the defect core, also showing the degree of biaxiality, is given in Fig. 2(a). There, we plot both r and β^2 across the defect in both z and y directions. At the defect center, $r=0$ and $\beta^2=0$. On increasing the distance $\rho=\sqrt{(y-y_{\mathrm{def}})^2+(z-z_{\mathrm{def}})^2}$ from the defect, the degree of biaxiality β^2 at first gradually increases; it reaches its maximum value $\beta^2=1$ for $\rho \sim \xi_b$. Upon further increasing ρ, the uniaxial ordering with $\beta^2=0$ is asymptotically approached. On the contrary, r correspondingly increases and finally saturates at a uniform value.

Thus, the defect center is uniaxial as in Ref. [8]. It is surrounded by a strong biaxial region, peaked at $\rho \sim \xi_b$, which approximately exhibits a cylindrical symmetry about the x axis through the point $(y_{\mathrm{def}},z_{\mathrm{def}})$. For $\rho \gg \xi_b$, an almost perfect uniaxial ordering is realized. Note that the apparent departure from the perfect cylindrical symmetry in Fig. 2(a) is due to the cell confinement along the z axis and to the approximate equality of d and ξ_b. As the ratio d/ξ_b increases, the core becomes gradually circular in the limit as $d/\xi_b \rightarrow \infty$.

For $E_a>0$, the established electric field tends to enforce a homogeneous nematic alignment along the z axis. Consequently, with increasing E_a the defect is pushed toward the bottom plate. We say that the defect is expelled from the cell when $z_{\mathrm{def}}=-d$, i.e., $r(0,-d)=0$. There are two qualitatively different expulsion scenarios, depending on the anchoring strength. If the surface anchoring strength is weak enough (i.e., $W/W_0 \lesssim 0.5$) then the line defect is expelled, accompanied by rather minor changes in the core configuration, as already shown by Biscari and Sluckin [21]. On the other hand, for strong enough anchorings, the defect exhibits dramatic changes in the core shape, as shown in Figs. 1(b)–1(e).

In the following, we limit our discussion to intermediate and strong anchorings, i.e., $W/W_0>0.5$, focusing attention on the surface biaxiality promoted by the defect. The core structure is relatively weakly influenced by E_a when the defect distance from the plate is larger than ξ_b. This is well shown in Fig. 2(b), where the core structures for $z_{\mathrm{def}}=0$ and $d-z_{\mathrm{def}}=0.15d \sim \xi_b$ are superimposed. For $E_a \lesssim E_c$ the nematic ordering within the main portion of the cell becomes mostly uniaxial, almost perfectly aligned along the z axis. At the same time the contrasting anchoring tendency at the cell plate tends to establish a biaxial layer of thickness $\sim \xi_b$ for strong enough values of E_a. For $d-z_{\mathrm{def}}<\xi_b$ the core structure and the surface biaxiality become apparently mutually affected, as shown in Figs. 1(c) and 1(d). In particular, Fig. 1(d) shows the interference between core and surface biaxialities.

The degree of surface induced biaxiality is sensitive to the presence of the defect. To quantify the influence of the surface on the defect structure, we follow in Fig. 3 the change in both the width ξ_y and height ξ_z of the defect core as the wall is approached. We formally define ξ_y and ξ_z as the distances along the y and z axes, respectively, between the defect center and the point where $\beta^2=1$. One sees that ξ_z is only slightly affected, while ξ_y diverges as the wall is approached. Therefore the contours representing the defect core become increasingly prolate in the y direction. Finally, the defect core merges with the biaxial layer and can no longer be distinguished from it [see Fig. 1(e)].

We henceforth refer to the configuration with a line defect as the LD texture. Upon increasing E_a, this texture is continuously transformed into a qualitatively different configu-

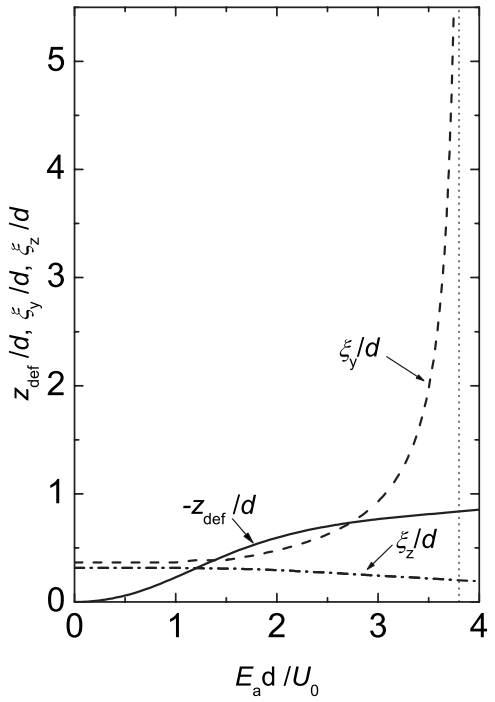

FIG. 3. Variation of the defect core size as z_{def} approaches the cell wall at $z=-d$. The lengths ξ_y and ξ_z estimate the core size along the y and z axes, respectively. $W/W_0=5$, $d/\xi_b=4$.

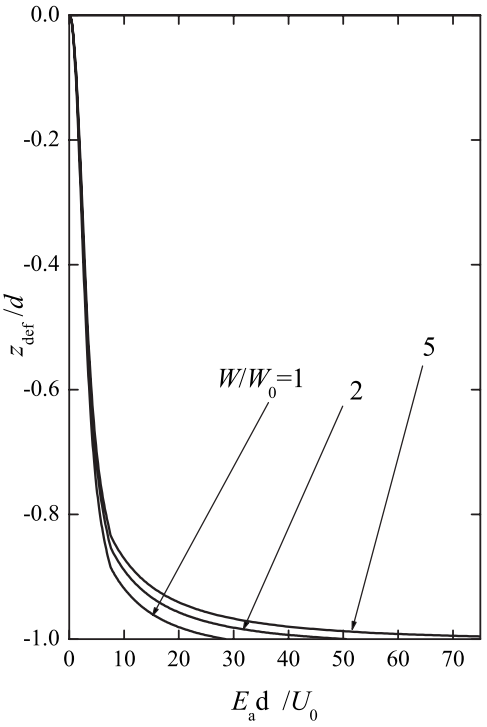

FIG. 4. The position of the line/plane defect as a function of E_a for different values of W; $d/\xi_b=8$.

ration at $E_a=E_c^*$. In the emerging texture, the tensor $\mathbf{Q}$ exhibits a diffused order reconstruction: its principal eigenvector $\mathbf{n}$ is perpendicular to the plates in the larger upper part of the cell, whereas it is parallel to the plates in the rest of the cell. These different regions are separated by a plane defect, on which $q_2=0$. We refer to this configuration as the plane defect (PD) texture. For later use, we also introduce the no defect (ND) texture. This texture is as compatible with the anchoring conditions as the LD texture and exhibits spatial deformation only along the z axis. For $E_a=0$, it is essentially uniaxial, and φ varies linearly between the plates. For a weak enough E_a, this texture corresponds to the global minimizer of the system.

The transition between the LD and PD textures is manifested in a change of slope in the graph of $z_{def}=z_{def}(E_a)$, as shown in Fig. 4. The steeper part of this graph reflects the movement of the line defect in the LD texture. At the threshold field $E_a=E_c^*$, the linear defect becomes a surface, planar biaxial layer. As E_a is increased above E_c^*, this plane defect gradually approaches the lower plate. Therefore for $E_a \gtrapprox E_c^*$ the nematic texture exhibits only spatial variations along the z axis. This is reflected by the decreased slope of the graph of $z_{def}=z_{def}(E_a)$. At the critical value $E_a=E_c>E_c^*$, the plane defect is eventually expelled from the cell.

The function $z_{def}=z_{def}(E_a)$ does not exhibit a qualitative change in behavior as W is varied, provided that $W/W_0>1$. For any given value of W, $z_{def}(E_a)$ exhibits two different regimes, characterized by a different degree of steepness in its graph. The critical value E_c monotonically increases with increasing anchoring strength, as shown in Fig. 5. We also checked the behavior of E_c as a function of the cell thickness d_z. For this purpose we calculated E_c for cells of thickness $d_z=8\xi_b$ and $d_z=16\xi_b$. We obtained the same E_c to within an accuracy better than 1%.

We further show that the line defect promotes the formation of a surface layer with a large degree of biaxiality as E_a is increased in the regime studied here. This phenomenon is universal and valid for a sufficiently strong anchoring, i.e.,

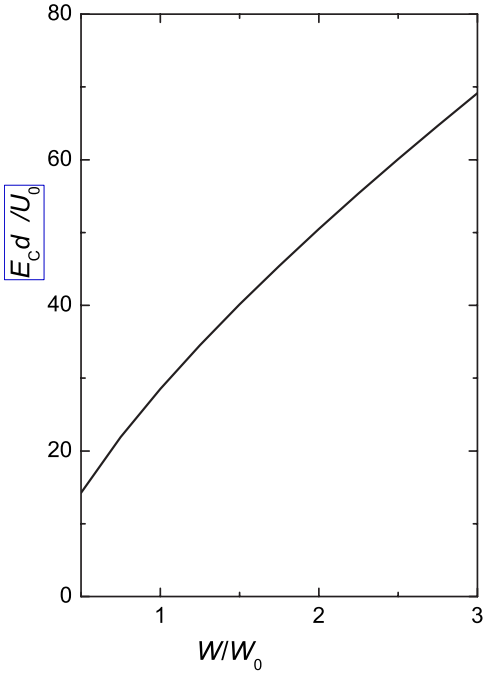

FIG. 5. (Color online) The critical potential E_c as a function of the anchoring strength W; $d/\xi_b=8$.

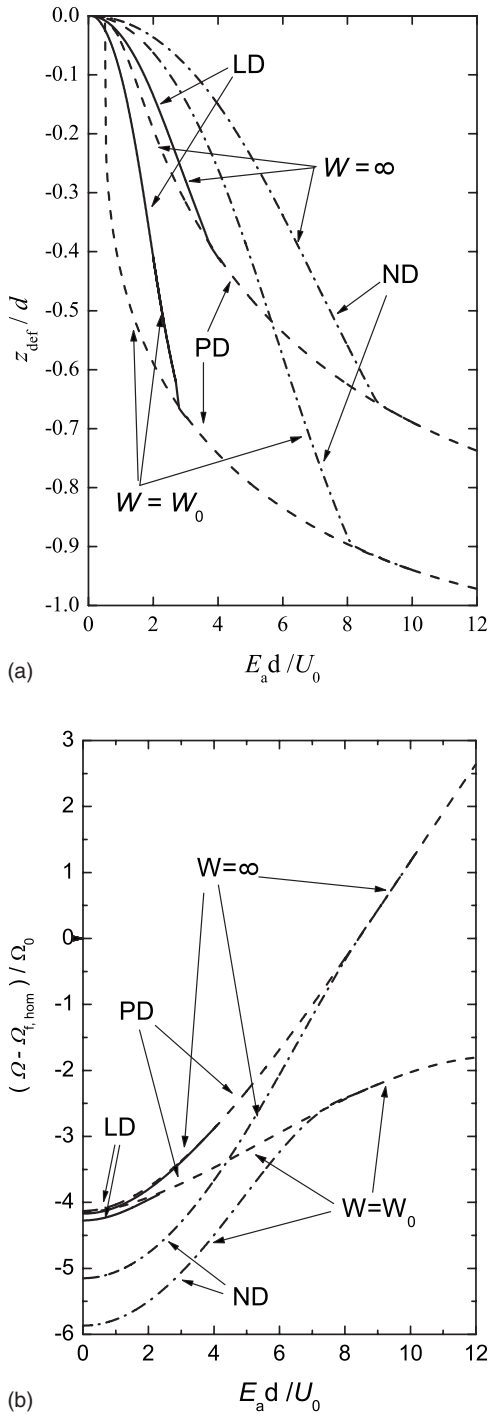

FIG. 6. The comparison between three qualitatively different nematic configurations: line defect (LD, solid lines), no defect (ND, dash-dotted lines), and plane defect (PD, dashed lines). (a) The z coordinate of the line/plane where $q_2=0$ plotted against $E_a d/U_a$. (b) The total free energy, deprived of the field contribution, plotted against $E_a d/U_a$. Here $d/\xi_b=4$ and $W/W_0=1$ or $W/W_0\to\infty$.

for $W/W_0 \gtrapprox 1$. To show this, we compare in Fig. 6 the evolution for increasing E_a of the three relevant textures: namely, LD (solid line), PD (dashed line), and ND (dash-dotted line). To emphasize the role of the PD texture in the defect-enhanced surface biaxiality, we calculate it for all values of E_a by enforcing $q_3=0$, that is, $\varphi=0$, and by prescribing a homogeneous texture in all planes parallel to (x,y). This texture exists and can be stable only for large enough values of E_a. Our numerical simulation suggests that below E_c^* the PD texture is either unstable or weakly metastable. To test its stability we relaxed the constraint $q_3=0$ in the PD texture, which then gradually transformed into the LD texture for $E<E_c^*$.

To monitor the characteristic structural changes we follow the position of the set where $q_2=0$ (either line or plane) as E_a is increased. Note that in the ND texture the plane $q_2=0$ identifies the surface with $\varphi=\frac{\pi}{4}$, in the LD texture it marks the position of the line defect, and in the PD texture it identifies the plane defect. We see that as E_a is increased, the LD and PD textures become identical at $E_a=E_c^*$, where $E_c^*\approx 2.8$ for $W=W_0$ and $E_c^*\approx 3.8$ as $W\to\infty$. Above this critical field the defect is transformed into a surface layer with large biaxiality. In the absence of defect, the formation of a surface layer takes place at higher voltages. Figure 6(a) shows that the PD and ND textures merge at the critical field $E_a=E_c^{**}$, where $E_c^{**}\approx 8$ for $W=W_0$ and $E_c^*\approx 8.8$ as $W\to\infty$. Thus, the difference between E_c^* and E_c^{**} is relatively large for any W, provided that $W/W_0 \gtrapprox 0.5$. Figure 6(b) compares the free energies of the three textures, revealing the continuous structural transitions LD-PD and ND-PD. In this figure we plot the excess free energy, where the contribution of the field on a texture homogeneously aligned along the z axis has been subtracted. This makes it easier to compare relatively small energy differences between the different textures involved.

The ND texture plays the role of a case of comparison: it is transformed into the PD texture when E_a reaches E_a^{**}; the surface plane defect thus formed is then expelled from the cell when E_a reaches E_c; in all cases studied here, $E_c^*<E_c^{**}<E_c$. For W sufficiently large and $E_c^{**}<E_a<E_c$, the surface biaxial layer bridges two uniaxial states, one homeotropic in the bulk and the other planar on the boundary, by an exchange of eigenvalues in the order tensor $\mathbf{Q}$ with fixed eigenvectors. In the present planar geometry, this phenomenon is known to happen in the bulk and it is often called the order reconstruction [28–33]. Our model suggests that a similar phenomenon could appear on surfaces with sufficiently strong anchoring. For $E_a \geqslant E_c^*$, the PD texture has in the bulk the same appearance as the ND texture for $E_a \geqslant E_c^{**}$. We could interpret the LD-PD transition as a "surface" order reconstruction induced by the line defect explosion.

IV. CONCLUSIONS

We studied the expulsion from a nematic cell of a line defect with topological charge $M=\pm\frac{1}{2}$, obtained by applying an external electric field. We focussed attention on the interplay between the defect and the surface. We adopted a Landau–de Gennes approach, formulated in terms of an order tensor. In the absence of the electric field, the defect was stable within a planar cell with plates enforcing hybrid boundary conditions. We assigned a uniaxial homeotropic anchoring at the top plate and a tangential uniaxial anchoring at the bottom plate; the anchoring strength was W at both plates. We considered the case where the curvature of the line defect is negligible on the scale comparable to the cell

thickness d_z. We further assumed that the local environment of the defect is dominated by the anchoring boundary conditions. Therefore a possible neighboring defect is farther from it than d_z. We applied an electric field along the cell's normal (precisely, along the z axis, while the defect was along the x axis) with average strength E_a; this field tended to expel the defect from the cell.

We showed that in the absence of the external field the biaxial defect core exhibits locally an almost circular cylindrical symmetry. The axis of the defect is uniaxial with a negative order parameter and it is surrounded by a cylinder characterized by the maximum degree of biaxial ordering ($\beta^2=1$). For a strong enough anchoring ($W/W_0 \gtrapprox 0.5$) and for equal anchoring strengths at both plates, the defect is centered in the middle of the cell. As the strength of the external field is increased, the defect progressively approaches the bottom plate. When the distance $d_{\mathrm{def}}=d-|z_{\mathrm{def}}|$ between this plate and the defect becomes comparable to the biaxial correlation length ξ_b, the defect starts to grow. While the size ξ_z of the core in the z direction remains essentially the same, the size ξ_y in the y direction monotonically increases with decreasing d_{def}. At $E_a=E_c^*$, the value of ξ_y diverges, signaling a nematic order reconstruction. At $E_a=E_c>E_c^*$, the surface reconstruction plane is expelled from the cell. We identified the critical threshold E_c^{**}, defined as the value of E_a at which the biaxial surface layer would be indifferently produced either by the plane defect squeezed by the field on the antagonistic surface or by a defectless texture.

For the set of material parameters used in our simulations we observed a nearly linear variation of the electric potential across the cell (i.e., an almost uniform electric field). The only slight departure from this behavior was observed in the neighborhood of the plane defect for $E_a>E_c^*$ in the vicinity of the bottom plate. A similar behavior was already found in the general, analytic study of the regime following Freedericksz's transition, performed in Ref. [34] under the assumption of strong anchoring. This regime was also studied by Mottram and Hogan [35], who showed that high fields can induce a partial surface melting.

A natural question is whether our simulation describes a realistic scenario within a typical hybrid cell with tangential anchoring on one plate and homeotropic anchoring on the other plate. Assume that the LC is quenched from the isotropic to the nematic phase within the cell. Soon after the quench, by symmetry breaking, line defects dominate the scene [36,37]. Individual defects that are not too close to one another tend to straighten up to equalize the elastic distortions in their vicinity. By topological and energetic reasons, the most probable scenario is a sequence of line defects in a given direction with alternating charges $M=\pm\frac{1}{2}$. For a strong enough anchoring, one such sequence, where the distance separating the defects is on average larger than the cell thickness, might get caught into a metastable state. In this case, the neighboring defects of opposite topological charge are elastically decoupled by the surface screening effect [38]. An applied electric potential on the cell plates also introduces a kind of screening effect because with increasing potential the region surrounding a defect becomes dominated by the imposed electric field. Our simulation describes reasonably well such an isolated and stabilized defect, where the x axis is set along the average local line defect orientation (on a scale comparable to the cell thickness).

The first conclusion of our paper is that a line defect is expelled by an electric field in two stages: first its core explodes into a biaxial wall, then, for higher field strengths, the wall is expelled. The second conclusion is that for fields strong enough, both in the presence and in the absence of defects, two competing anchorings can be bridged by surface order reconstruction. Both types of surface order reconstructions have been observed experimentally [39] and simulations have been conducted on the absorption of a bulk biaxial wall onto a bounding surface [40]. Here we gave a proof of principle that the presence of defects lowers the threshold for surface order reconstruction.

ACKNOWLEDGMENTS

We thank R. Barberi for having disclosed his results [39,40] prior to publication and G. E. Durand for a critical reading of this paper.

APPENDIX: EULER-LAGRANGE EQUATIONS

The bulk equilibrium equations in the dimensionless parametrization of the free energy functional adopted here read as

$$q_{i,yy}+q_{i,zz}+g_i+h_i=0, \quad i=1,2,3, \tag{A1}$$

where

$$g_1=\frac{1}{\xi_0^2}\left\{-\frac{\theta q_1}{6}+\frac{q_2^2+q_3^2-3q_1^2}{3}-\frac{q_1(3q_1^2+q_2^2+q_3^2)}{2}\right\}, \tag{A2a}$$

$$g_2=\frac{1}{\xi_0^2}\left\{-\frac{\theta q_2}{6}+2q_1q_2-\frac{q_2(3q_1^2+q_2^2+q_3^2)}{2}\right\}, \tag{A2b}$$

$$g_3=\frac{1}{\xi_0^2}\left\{-\frac{\theta q_3}{6}+2q_1q_3-\frac{q_3(3q_1^2+q_2^2+q_3^2)}{2}\right\}, \tag{A2c}$$

$$h_1=\frac{\varepsilon_a}{6t}(U_{,y}^2+U_{,z}^2), \tag{A2d}$$

$$h_2=\frac{\varepsilon_a}{2t}(-U_{,y}^2+U_{,z}^2), \tag{A2e}$$

$$h_3=\frac{\varepsilon_a}{t}U_{,y}U_{,z}. \tag{A2f}$$

The surface equilibrium equations for q_i at the bottom plate ($z=-1$) are

$$q_{1,z}-\frac{W}{\xi_0^2}\left(q_1-\frac{t}{6}\right)=0, \tag{A3a}$$

$$q_{2,z}-\frac{W}{\xi_0^2}\left(q_2+\frac{t}{2}\right)=0, \tag{A3b}$$

$$q_{3,z} - \frac{W}{\xi_0^2} q_3 = 0. \tag{A3c}$$

The corresponding equations at the top plate ($z=1$) are

$$q_{1,z} + \frac{W}{\xi_0^2}\left(q_1 - \frac{t}{6}\right) = 0, \tag{A4a}$$

$$q_{2,z} + \frac{W}{\xi_0^2}\left(\frac{q_2}{t} - \frac{t}{2}\right) = 0, \tag{A4b}$$

$$q_{3,z} + \frac{W}{\xi_0^2} q_3 = 0. \tag{A4c}$$

In the strong anchoring limit as $W \to \infty$, it follows from Eqs. (A3) and (A4) that correspondingly $q_1(\pm 1) \to t/6$, $q_2(\pm 1) \to \pm t/2$, $q_3(\pm 1) \to 0$.

The bulk differential equation for the electric potential, following from the condition that div $\mathbf{E}=0$, is given by

$$[1 + \varepsilon_a(q_1 - q_2)]U_{,yy} + [1 + \varepsilon_a(q_1 + q_2)]U_{,zz} + 2\varepsilon_a q_3 U_{,yz} + h_u = 0, \tag{A5}$$

where

$$h_u = \varepsilon_a(q_{1,y} - q_{2,y} + q_{3,z})U_{,y} + \varepsilon_a(q_{1,z} + q_{2,z} + q_{3,y})U_{,z}. \tag{A6}$$

At the plates the potential is prescribed as $U|_{z=\pm 1} = \pm U_a$.

[1] M. Kleman, *Points, Lines and Walls: in Liquid Crystals, Magnetic Systems and Various Disordered Media* (Wiley, New York, 1983).
[2] C. Denniston and J. Yeomans, Phys. Rev. Lett. **87**, 275505 (2001).
[3] N. Mermin, Rev. Mod. Phys. **51**, 591 (1979).
[4] T. W. B. Kibble, J. Phys. A **9**, 1387 (1976).
[5] F. C. Frank, Discuss. Faraday Soc. **25**, 19 (1958).
[6] M. V. Kurik and O. D. Lavrentovich, Usp. Fiz. Nauk **154**, 381 (1988) [Sov. Phys. Usp. **31**, 196 (1988)].
[7] P. G. de Gennes and J. Prost, *The Physics of Liquid Crystals* (Oxford University Press, Oxford, 1993).
[8] N. Shopohl and T. J. Sluckin, J. Phys. (France) **49**, 1097 (1988).
[9] R. Rosso and E. G. Virga, J. Phys. A **29**, 4247 (1996).
[10] E. C. Gartland and S. Mkaddem, Phys. Rev. E **59**, 563 (1999).
[11] S. Kralj, E. G. Virga, and S. Žumer, Phys. Rev. E **60**, 1858 (1999).
[12] S. Kralj, S. Žumer, and D. W. Allender, Phys. Rev. A **43**, 2943 (1991).
[13] E. Penzenstadler and H. R. Trebin, J. Phys. (France) **50**, 1025 (1989).
[14] P. Biscari, G. G. Peroli, and T. J. Sluckin, Mol. Cryst. Liq. Cryst. Sci. Technol., Sect. A **292**, 91 (1997).
[15] N. Schopohl and T. J. Sluckin, Phys. Rev. Lett. **59**, 2582 (1987).
[16] R. Meyer, Mol. Cryst. Liq. Cryst. **16**, 355 (1972).
[17] R. Meyer, Solid State Commun. **12**, 585 (1973).
[18] V. G. Bodnar, O. D. Lavrentovich, and V. M. Pergamenshchik, Zh. Eksp. Teor. Fiz. **101**, 111 (1992) [Sov. Phys. JETP **47**, 61 (1992)].
[19] S. Kralj and E. G. Virga, Phys. Rev. E **66**, 021703 (2002).
[20] P. Biscari and T. J. Sluckin, SIAM J. Appl. Math. **65**, 2141 (2005).
[21] P. Biscari and T. J. Sluckin, Eur. J. Appl. Math. **14**, 39 (2003).
[22] R. Rosso and M. C. P. Brunelli, Continuum Mech. Thermodyn. **13**, 383 (2001).
[23] O. D. Lavrentovich and S. S. Rozhkov, Pis'ma Zh. Eksp. Teor. Fiz. **47**, 210 (1988) [JETP Lett. **47**, 254 (1988)].
[24] E. G. Virga, *Variational Theories for Liquid Crystals* (Chapman Hall, London, 1994).
[25] P. Kaiser, W. Wiese, and S. Hess, J. Non-Equilib. Thermodyn. **17**, 153 (1992).
[26] F. Bisi, E. C. Gartland, R. Rosso, and E. G. Virga, Phys. Rev. E **68**, 021707 (2003).
[27] W. Press, B. Flannery, S. Teukolsky, and W. Vetterling, *Numerical Recipies* (Cambridge University Press, Cambridge, 1986).
[28] P. Martinot-Lagarde, H. Dreyfus-Lambez, and I. Dozov, Phys. Rev. E **67**, 051710 (2003).
[29] R. Barberi, F. Ciuchi, G. Durand, M. Iovane, D. Sikharulidze, A. Sonnet, and E. G. Virga, Eur. Phys. J. E **13**, 61 (2004).
[30] R. Barberi, F. Ciuchi, G. Lombardo, R. Bartolino, and G. E. Durand, Phys. Rev. Lett. **93**, 137801 (2004).
[31] S. Joly, I. Dozov, and P. Martinot-Lagarde, Phys. Rev. Lett. **96**, 019801 (2006).
[32] R. Barberi, F. Ciuchi, H. Ayeb, G. Lombardo, R. Bartolino, and G. E. Durand, Phys. Rev. Lett. **96**, 019802 (2006).
[33] Y. Zhang, B. Wang, D. B. Chung, J. Colegrove, and P. J. Bos, SID Proc. **36**, 1782 (2005).
[34] R. H. Self, C. P. Please, and T. J. Sluckin, Eur. J. Appl. Math. **13**, 1 (2002).
[35] N. J. Mottram and S. J. Hogan, Continuum Mech. Thermodyn. **14**, 281 (2002).
[36] A. N. Pargellis, J. Mendez, M. Srinivasarao, and B. Yurke, Phys. Rev. E **53**, R25 (1996).
[37] Z. Bradač, S. Kralj, and S. Žumer, Phys. Rev. E **65**, 021705 (2002).
[38] A. Bogi, P. Martinot-Lagarde, I. Dozov, and M. Nobili, Phys. Rev. Lett. **89**, 225501 (2002).
[39] H. Ayeb, F. Ciuchi, G. Lombardo, R. Barberi, and G. Durand (unpublished).
[40] G. Lombardo, H. Ayeb, and R. Barberi (unpublished).